Wind and Structures, *Vol. 22, No. 2 (2016) 185-209*
DOI: http://dx.doi.org/10.12989/was.2016.22.2.185

Effects of turbulence intensity and exterior geometry on across-wind aerodynamic damping of rectangular super-tall buildings

Y. Quan[a], H.L. Cao[b] and M. Gu[*]

State Key Laboratory of Disaster Reduction in Civil Engineering, Tongji University, Shanghai 200092, China

(Received April 15, 2014, Revised October 12, 2015, Accepted December 14, 2015)

Abstract. Across-wind aerodynamic damping ratios are identified from the wind-induced acceleration responses of 15 aeroelastic models of rectangular super-high-rise buildings in various simulated wind conditions by using the random decrement technique. The influences of amplitude-dependent structural damping ratio and natural frequency on the estimation of the aerodynamic damping ratio are discussed and the identifying method for aerodynamic damping is improved at first. Based on these works, effects of turbulence intensity I_u, aspect ratio H/B, and side ratio B/D on the across-wind aerodynamic damping ratio are investigated. The results indicate that turbulence intensity and side ratio are the most important factors that affect across-wind aerodynamic damping ratio, whereas aspect ratio indirectly affects the aerodynamic damping ratio by changing the response amplitude. Furthermore, empirical aerodynamic damping functions are proposed to estimate aerodynamic damping ratios at low and high reduced speeds for rectangular super-high-rise buildings with an aspect ratio in the range of 5 to 10, a side ratio of 1/3 to 3, and turbulence intensity varying from 1.7% to 25%.

Keywords: high-rise building; aerodynamic damping; aeroelastic model; wind tunnel test; wind-induced vibration

1. Introduction

Aerodynamic damping usually plays an important role in wind-induced vibrations of super-tall buildings, especially Kareem (1978) revealed the significance of across-wind aerodynamic negative damping. In fact, great efforts have been made on this problem. Steckley (1989), Steckley *et al*. (1990) and Vickery and Steckley (1993) estimated the aerodynamic damping ratios at various reduced wind speeds from forced oscillation experiments for building models with various tip deflections, turbulence intensities, and aspect ratios by using the swept frequency method. Moreover, variation curves of the aerodynamic damping ratio versus reduced wind speeds for building models with various cross sections, such as circular, triangular, square cross-section with chamfered corners, and rectangular, were provided. Notably, the turbulence intensity was also

*Corresponding author, Professor, E-mail: minggu@tongji.edu.cn
[a] Professor, E-mail: quanyong@tongji.edu.cn
[b] Ph.D., E-mail: mmchl_132@163.com

http://www.techno-press.org/?journal=was&subpage=8 ISSN: 1226-6116 (Print), 1598-6225 (Online)

changed when the aspect ratio was changed. Thus, these studies failed to investigate the effect of aspect ratio individually. Watanabe *et al.* (1997) proposed an empirical aerodynamic damping function for tall buildings and prisms based on the wind tunnel test results of Steckley (1989). A number of physical conditions, such as tip deflection, aspect ratio, the shape of a building's cross section, and the turbulence intensity of incident flow are involved to the aerodynamic damping function. Nishimura *et al*. (1995) reported the characteristics of aerodynamic damping of a tall square building by forcing two models, which were placed separately inside and outside the wind tunnel, to perform harmonic oscillations simultaneously. Marukawa *et al*. (1996) evaluated the aerodynamic damping ratios of tall rectangular buildings from the wind tunnel tests of aeroelastic models. The effects of side ratio, aspect ratio, and structural damping ratio on across-wind aerodynamic damping ratio were analyzed by using the random decrement technique (RDT). Similar to the study by Steckley (1989), the effect of aspect ratio was failed to be examined individually because turbulence intensity was changed with the change of aspect ratio. Cheng *et al*. (2002) compared the wind-induced responses of the aeroelastic model with responses predicted with the wind forces on a rigid model. The characteristics of across-wind response and aerodynamic damping ratio weres studied and finally empirical models for aerodynamic damping was proposed. Zou *et al*. (2003) used the RDT method to examine the variation of across-wind aerodynamic damping ratios of a rectangular building with a side ratio of 2:1 at three reduced wind speeds. Quan *et al*. (2002, 2004, 2005) and Gu and Quan (2004) investigated the effects of reduced wind speed, structural damping ratio, and turbulence intensity on across-wind aerodynamic damping ratio for tall square buildings. Venanzi and Materazzi (2012) studied on prediction of the acrosswind aeroelastic responses of square tall buildings. Li *et al*. (2014) investigate the effects of turbulence integral length scale and turbulence intensity on the along-wind responses, across-wind responses and torsional responses of the tall building by Large Eddy Simulation. Kim *et al*. (2015) investigate the effect of taper on fundamental aeroelastic behaviors of super-tall buildings in various incident flows with an aeroelastic model wind tunnel test.

In summary, only a few studies have focused on the effects of turbulence intensity, aspect ratio, and side ratio on the across-wind aerodynamic damping ratio of a super-high-rise building, which are far from systemization and lack of comparisons among research achievements. As a result, consistent and comprehensive rules have not been obtained. According to Cao (2012), across-wind aerodynamic damping ratio at low reduced wind speed is inversely proportional to tip deflection, while across-wind aerodynamic damping ratio at high reduced wind speed is greatly related to the aerodynamic stability. However, existing aeroelastic experimental studies do not consider directly the effect of tip deflection for across-wind aerodynamic damping ratios.

In the present study, across-wind aerodynamic damping ratios are determined from the wind-induced responses of 15 aeroelastic models in nine simulated wind flow conditions at first, and then the influences of amplitude-dependent structural damping ratio and natural frequency on the estimation of the aerodynamic damping ratio are discussed. The effects of turbulence intensity, aspect ratio, and side ratio on the across-wind aerodynamic damping ratios of super-high-rise buildings are investigated and corresponding empirical functions are proposed at last.

2. Outline of the wind tunnel tests

2.1 Simulation of wind characteristics

The aeroelastic model tests of super-high-rise buildings were conducted in the TJ-1 Boundary Layer Wind Tunnel at Tongji University, China. The TJ-1 Boundary Layer Wind Tunnel is an open circuit wind tunnel. Its working section is 1.8 m in width, 1.8 m in height, and 18 m in length. Its working wind speed ranges from 3 m/s to 32 m/s. Nine types of exposures, corresponding to terrain category B in the Chinese code (GB50009-2012), as well as eight other exposures for the investigation of effect of exposure (longitudinal turbulence intensity) on aerodynamic damping ratio, were simulated in the wind tunnel at a length scale of 1/800. Fig. 1 shows the simulated mean wind speed profiles, the profiles of the turbulence intensity, and the power spectral densities (PSDs) of the fluctuating wind speed at the model height. The corresponding mean wind speed profile provided by the Chinese code and the turbulence intensity profile given by the Architectural Institute of Japan (AIJ 2004) for terrain category B are also shown in Fig. 1. According to the Chinese code, the exponent of the mean wind speed profile for terrain category B is 0.16. The exponents of the mean wind speed profiles for the other eight exposures are 0.06, 0.06, 0.13, 0.16, 0.18, 0.20, 0.21 and 0.23, separately. For terrain category B, longitudinal turbulence intensity at the model height is 9.36% in accordance with AIJ (2004). The simulated longitudinal turbulence intensities at the model heights for the other eight exposures are respectively 1.7%, 4.6%, 7.4%, 9.4%, 10.9%, 13.7%, 17.4%, and 24.9%. A precise simulation of the integral scale of turbulence in wind tunnel tests is always difficult to achieve. In present study, the integral scale of turbulence for terrain category B is 231 m at two-thirds the building height. Meanwhile, the integral scales of turbulence for the other eight exposures at two-thirds the building height are 270, 160, 380, 360, 370, 420, 470 and 240 m, respectively. The integral scales of turbulence simulated for all the exposures are larger than the building width and fall in the range of field-measured results provided in AIJ (2004). The parameters of the simulated wind fields are listed in Table 1 also, in which a, I_u and L_u are the exponent of the mean wind speed profile, longitudinal turbulence intensity at the model height and the longitudinal turbulence integral scale at two-thirds the building height, respectively.

The height of the target buildings is 600 m, which is higher than the gradient height defined in most standards. The wind speed above "gradient height" is not given in the standards of USA (ASCE/SEI 7-10), Europe (preEN 1991-1-4) and Japan (AIJ 2004), while it increases up to the height of 1000 m with power law in International Standard(ISO 4354) and it is a fixed value in Chinese standard (GB50009-2012). In the present study, it is assumed that the wind speed increase up to the building heights, which is the same as the definition in ISO4354.

2.2 Building models

Firstly we chose a standard case of super-high-rise buildings in the study. In this study, the turbulence intensity, aspect ratio and side ratio were independently varied in turn to investigate the effect of individual parameter on across-wind aerodynamic damping ratio.

Table 1 Parameters of tested wind fields

No.	B	I	*II*	III	IV	V	VI	VII	VIII
α	0.16	0.06	0.06	0.13	0.16	0.18	0.20	0.21	0.23
I_u	9.4%	1.7%	4.6%	7.4%	9.4%	10.9%	13.7%	17.4%	24.9%
L_u	231 m	270 m	160 m	380 m	360 m	370 m	420 m	470 m	240 m

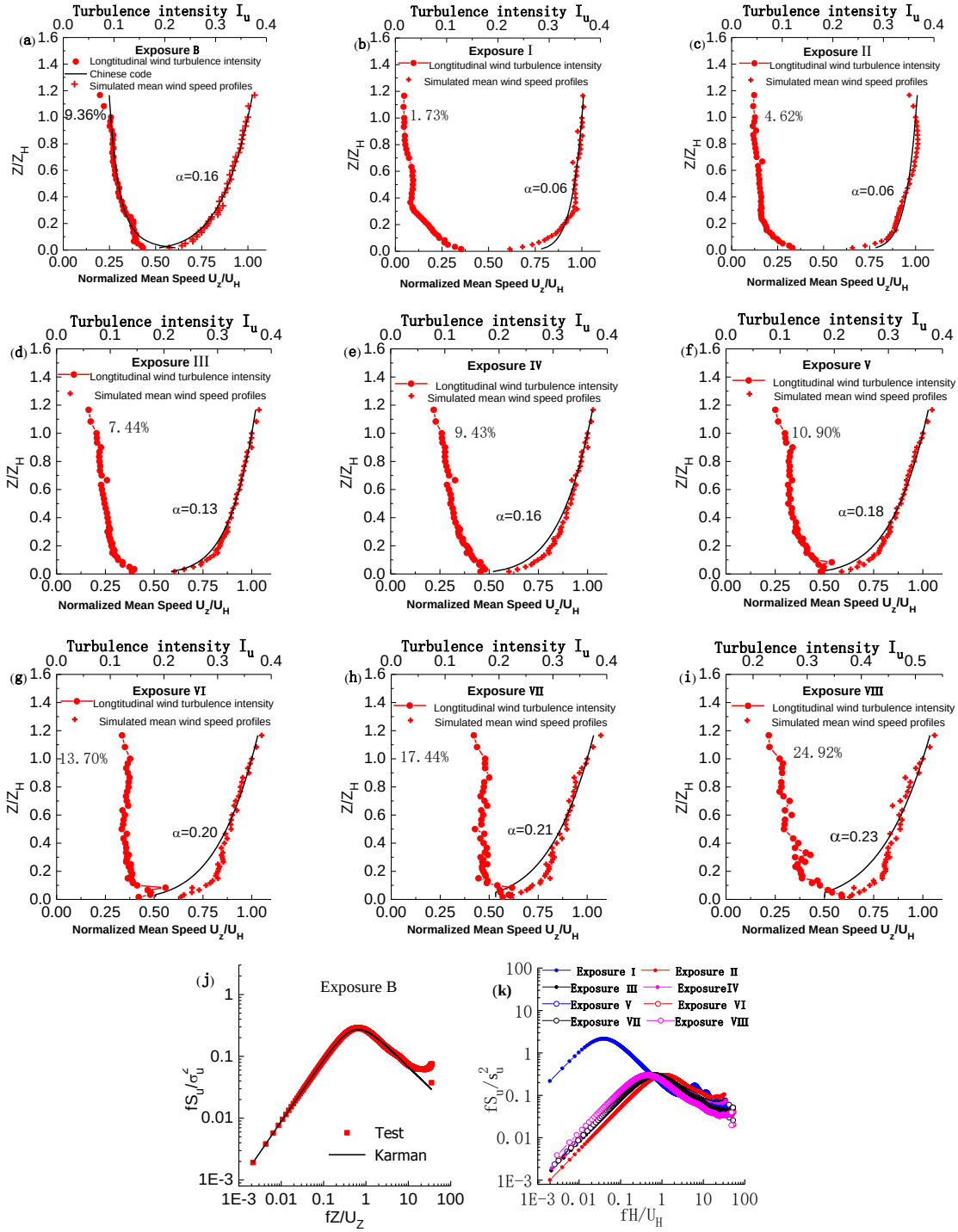

Fig. 1 Simulated wind speed profile(a-i), turbulence intensity profile(a-i) and PSD(j-k) of approching wind at buiding height

Table 2 Wind tunnel test cases for rectangular super-high-rise buildings

Case	Model Height H(mm)	Roughness Exposure	Side Ratio B/D	Aspect Ratio H/B	Mean Structural Damping Ratio ζ_s (%)	Mass Density ρ_s (Kg/m^3)	Generalized Stiffness K (Kg/s^2)
1–8	600	I-VIII	1	8	1.1	213	1600
9–13	600	B	1/3, 1/2, 1, 2, 3	8	1.1	213	1600
14–15	600	B	1	5, 10	1.1	213	1600

The dimensions of the prototype structure of the chosen standard case were 480 m × 60 m × 60 m (H × B × D), with a frequency of 0.13 Hz, a density of 213 Kg/m3, and a structural damping ratio of 1% in terrain category B (9.36% turbulence intensity of incident flow at building height). Reasonably considering the size of the wind tunnel test section, blockage area ratio, vortex shedding frequency, and the maximum working wind speed of the wind tunnel, the length scale and wind speed scale were chosen as 1/800 and 1/8, respectively. Corresponding to the test model of the chosen standard case, these parameters represented a model with a size of 0.6 m × 0.075 m × 0.075 m (1.39% blockage area ratio), a frequency of 13 Hz, a generalized mass of 0.24 Kg, a generalized stiffness of 1600 Kg/s^2, and a structural damping ratio of 1%. The height of the other model cases was the same as that of the standard model case, while the exterior geometries of the models were changed according to various aspect ratios and side ratios, as shown in Table 2. Among them, case 11 is the standard model case.

Fig. 2 Model base

Fig. 3 Standard Model Case

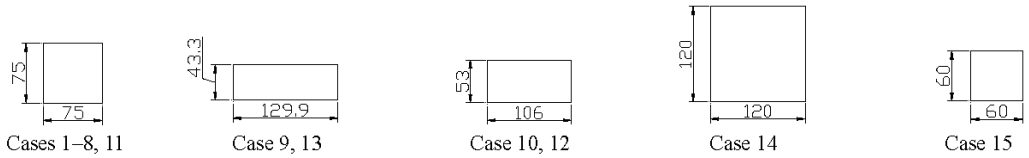

Fig. 4 Cross sections of building models (unit:mm)

The model base, the standard model case and cross sections of all the building models are shown in Figs. 2-4, respectively. The model base was used to simulate the elastic and damping parameters of the building. The structural damping ratio can be simulated by adjusting the width of the damping plates and their depth dipped into oil, while springs were used to achieve the stiffness required. To avoid energy transmission in the two orthogonal directions, one unconcerned degree of freedom in the horizontal direction was fixed in the tests. All the models were built with base plates, hollow aluminum alloy as cores, foamed plastics, light wood plates of 1 mm thickness as their "clothes" and balancing weights. The wind-induced acceleration responses of super-high-rise buildings with 15 kinds of structural properties were measured from the aeroelastic model wind tunnel test. Two piezoelectric accelerometers with a sampling frequency of 1000 Hz were placed at the top of the models. The sampling time was 7 mins.

3. Methodology

3.1 Estimation of aerodynamic damping ratio

The generalized RDT equation with four variables proposed by Tamura *et al*. (1996) was adopted to estimate the structural and aerodynamic damping ratios from the time series of random acceleration responses.

$$a(\tau) = Ae^{-\zeta_s \omega_0 \tau}\left(\cos\sqrt{1-\zeta_s^2}\,\omega_0\tau + B\sin\sqrt{1-\zeta_s^2}\,\omega_0\tau\right) \tag{1}$$

where A, B, ω_0 ($\omega_0=2\pi f_0$), and ζ_s are the four variables, while A and B denote the dummy variables that can be precisely estimated at the cost of processing time.

The variation curve of structural damping ratio with vibration amplitude was derived from free attenuation acceleration response under impulse excitation at first, and then the root mean square (RMS) of the wind-induced acceleration response after band-pass filtering was taken as the initial amplitude of RDT to extract the random decrement signature, which was used to estimate total damping ratio ζ. Subsequently, the structural damping ratio corresponding to this amplitude was derived by interpolation. The aerodynamic damping ratio ζ_a was calculated by subtracting the structural damping ratio ζ_s from the total damping ratio ζ, i.e., $\zeta_a = \zeta - \zeta_s$. In this process, the filtering bandwidth was $f \in (f_0^2/(f_s/16 \times f_0/f_{sm}), f_s/16 \times f_0/f_{sm})$, where f_s is the sampling frequency, while f_0 and f_{sm} are the natural frequency of the tested vibration model and the standard model, separately.

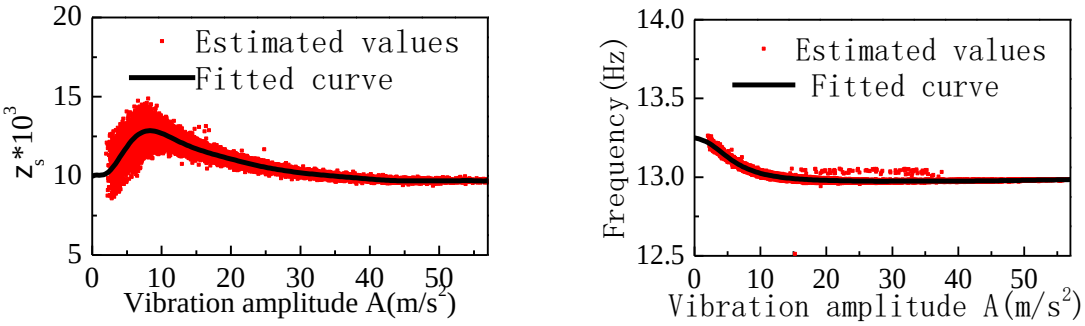

Fig. 5 Amplitude-dependent structural damping and frequency

3.2 Amplitude dependence of structural damping ratio

Before the wind tunnel test, the free decay time series of acceleration of the model were obtained from an impact vibration test. Every two continuous cycles of the free decay time series of acceleration were used to evaluate the structural damping ratio and natural frequency by using the least square method. Fig. 5 presents these results of the standard model case (i.e., Case 11 in Table 2, as an example. The variation tendency is consistent with the field measured structural damping ratios of real tall buildings provided by Tamura *et al*. (2000, 2006) and the experiment results given by Okada *et al*. (1993) and Aquino *et al*. (2011). Furthermore, also as an example, Fig. 6 shows the variation of the RMS of the wind-induced acceleration response of the standard model top with reduced wind speed. The results of all the tested models similar to Fig. 6 will be adopted in later sections for identification of aerodynamic damping.

For most super-high-rise buildings, the design reduced wind speeds are generally less than 10. As shown in Fig. 6, the RMS of the wind-induced acceleration response at the reduced wind speed of 10 is approximately 20 m/s^2. A combination of Figs. 5-6 shows that the structural damping ratio and frequency are obviously affected by the vibration amplitude when the acceleration response at the model height is less than 20 m/s^2. If structural damping ratio and vibration frequency of the models are taken as constants (for example, 1% and 13 Hz, respectively, for the standard model case) without considering the influence of vibration amplitude on structural damping and frequency in detail, misunderstandings on the variation of aerodynamic damping ratio with reduced wind speed will be developed.

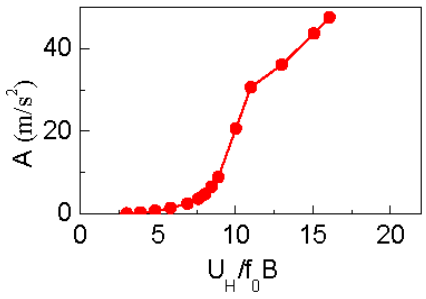

Fig. 6 RMS of wind-induced acceleration response

Therefore, the structural damping ratio as a function of the RMS of the wind-induced acceleration was adopted in the identification procedure of the aerodynamic damping. In this way, aforementioned misunderstandings could be avoided.

3.3 Selection of random decrement signature length

Considering the effects of vibration amplitude, the total damping ratio is also discrepant when different cycles of random decrement signatures are taken for its evaluation. Fig. 7 shows the effects of the amplitude dependence of the structural damping ratio and frequency on the aerodynamic damping ratio. As shown in Fig. 7, taking the amplitude dependence of structural damping ratio and frequency into consideration, positive and negative peak values of aerodynamic damping ratio occur at lower reduced wind speeds. Moreover, less cycles of the attenuation curve used for the estimation of the damping ratio also induces positive and negative peak values of the aerodynamic damping ratio to occur at lower reduced wind speeds because of the amplitude dependence of the structural damping ratio. Thus, in this paper, the first two cycles of the attenuation curves are chosen to estimate the damping ratios.

3.4 Verification of results

The experimental results in this paper were compared with those of previous research achievements, as shown in Fig. 7. Table 3 shows the experimental parameters. As shown in Table 3 and Fig. 7, the across-wind aerodynamic damping ratio is generally positive at low reduced wind speed and is negative at high reduced wind speed. The aerodynamic damping ratio rapidly changes from a positive peak to a negative peak in a specific range of reduced wind speeds. The remarkable differences among these results are mainly the discrepancies in the magnitudes of the peaks, the reduced wind speeds for the positive and negative peaks, and the critical reduced wind speeds at which the positive value of aerodynamic damping ratio become negative value.

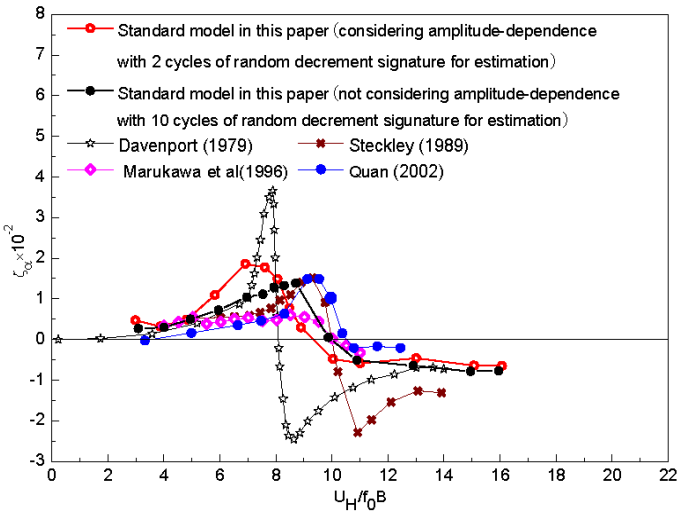

Fig. 7 Comparison of research achivements

Table 3 Experimental parameters

	Aspect Ratio *H/B*	Side Ratio *B/D*	Roughness Exposure (α, I_h)	Model Height *H* (*mm*)	Length Scale	Structural Damping Ratio ζ_s	Mass Density ρ_s (Kg/m^3)	Experimental Method
Test Standard Model	8	1	$\alpha = 0.16$ $I_h = 9.36\%$	600	1/800	1%	213	Random excitation method
Davenport (1979)	4.4	1	$\alpha = 0.32$ $I_h = 0.8\%$	660	/	/	adopt 182 here	Forced oscillation method
Steckley (1989)	13.3	1	$\alpha = 0.115$ $I_h = 6\%$	508	/	/	adopt 147 here	Forced oscillation method
Marukawa *et al*. (1996)	6	1	$\alpha = 0.167$ $I_h = 10.7\%$	480	1/500	1%	200	Random excitation method
Quan (2002)	6	1	$\alpha = 0.22$ Ih = 10%	600	1/500	1.2%	180	Random excitation method

The maximum magnitudes of the positive and negative peaks are presented by Davenport (1979). The results in this paper and those presented by Steckley (1989) and Quan (2002) have similar positive peaks. Marukawa *et al*. (1996) has the smallest positive peak. The negative peak given by Steckley (1989) is slightly smaller than that given by Davenport (1979), whereas those in other studies have similar negative peaks. The smallest reduced wind speeds correspond to the positive and negative peaks are provided by Davenport (1979), followed by the results considering the amplitude dependence in this paper. The reduced wind speeds correspond to the positive and negative peaks in other studies, including those without considering amplitude dependence in this paper, are close to one another. The critical reduced wind speed, at which the positive value of aerodynamic damping ratio become negative value, shows the same tendency as the reduced wind speeds for positive and negative peaks.

The reasons for the observed differences can be explained in the following aspects: (1) Different structural properties (mass, stiffness and structural damping) and geometries (aspect ratio, side ratio and height) make the peak values (positive and negative peaks) and critical reduced wind speeds in the studies discrepant from one another. For tall slender structures, the peaks of the aerodynamic damping ratio are relatively larger and the critical reduced wind speed is lower. The standard model in this paper has an aspect ratio of 8 while it is 6 in Quan (2002). Therefore, compared with the results given by Quan (2002), the present results indicate larger peaks and lower critical reduced wind speed. (2) Different turbulence intensities also cause discrepant peak values and critical reduced wind speed. Generally, the magnitudes of the peaks decrease as turbulence intensities increase, and the critical reduced wind speeds increase with turbulence intensities. The turbulence intensity of the simulated wind condition in Davenport (1979) is 0.8%, close to that of the smooth boundary, which induces the critical reduced wind speed evidently lower than the values obtained in other studies and makes both the positive and negative peaks the largest. (3) The negative peaks of the aerodynamic damping ratios obtained from the forced vibration tests are significantly larger than those derived from the random vibration of the aeroelastic models. A possible reason is that the tip deflections for a forced vibration test are

remained a constant at all reduced wind speeds, but the responses in the vicinity of the negative peaks are significantly larger than those in the range of the positive aerodynamic damping for an aeroelastic model test. (4) The results without considering amplitude dependence in the present study are close to the results given by Marukawa *et al*. (1996) and Quan (2002). When the effects of vibration amplitude on structural damping ratio and natural frequency were considered carefully, different features were observed for the aerodynamic damping ratio. This phenomenon further reveals a misunderstanding of the variation of the aerodynamic damping ratio with reduced wind speed will occur if the amplitude dependence of the structural damping ratio and the natural frequency of the aeroelastic model are neglected in damping estimation. However, no previous studies have emphasized this issue.

In summary, although discrepancies exist in the results because of different wind flow conditions, model parameters, and experimental methods from different researchers, the gross features of the present results are in agreement with the findings of previous studies and reasonable explanations for these discrepancies are provided. In addition, the reduced wind speed $U_H/(f_0B)$ in the aeroelastic model tests conducted by previous researchers is generally less than 13, and the structural damping ratio ζ_s is less than 2%. While this paper specifically studied the variation of the aerodynamic damping ratios of aeroelastic models at relatively high reduced wind speeds.

4. Characteristics of aerodynamic damping ratio

The aerodynamic damping ratios of the model cases in Table 2 are identified based on the methodology presented in Section 3. The effects of exposure (turbulence intensity I_u), aspect ratio H/B and side ratio B/D on the across-wind aerodynamic damping ratios of rectangular super-high-rise buildings are discussed in following section.

4.1 Effect of exposure

Fig. 8(a) shows the variations of aerodynamic damping ratio ζ_a with reduced wind speed U_H/f_0B for an aspect ratio H/B of 8 and a side ratio B/D of 1 in exposures I to VIII.

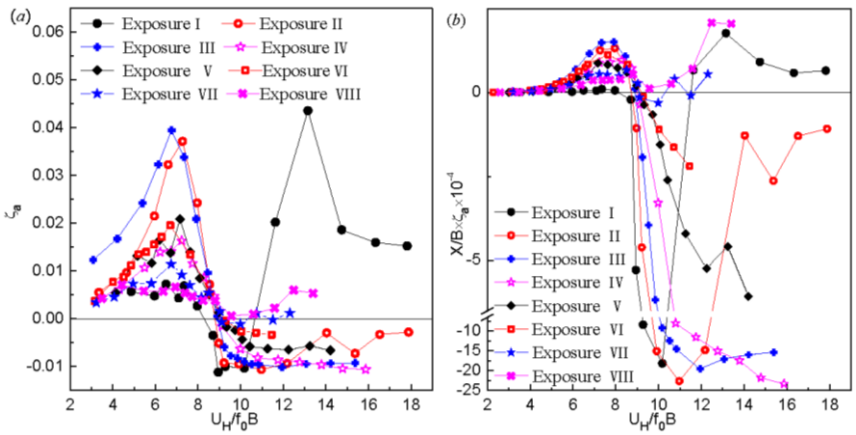

Fig. 8 Effect of roughness exposure on across-wind aerodynamic damping ratio ζ_a

For reduced wind speeds lower than 8, the magnitude of the positive peak of the aerodynamic damping ratio in exposure I is close to that in exposure VIII. When the reduced wind speed is varied from 7 to 10, the aerodynamic damping ratio in exposure I undergoes a rapid sign change from a positive peak to a negative peak. The magnitude of the negative peak in exposure I is the largest among all the tested exposure cases. At about reduced wind speed of 11, the aerodynamic damping ratio changes from negative value to positive value and it reaches a positive peak in the vicinity of a reduced wind speed of 14 in exposure I, which is also the maximum of the positive peak at all reduced wind speeds for all tested exposure cases. In exposure II, the magnitude of the positive peak of the aerodynamic damping ratio at a reduced wind speed lower than 8 is significantly larger than that in exposure I. When the reduced wind speed is varied from 7 to 12, the aerodynamic damping ratio undergoes a rapid sign change from a positive peak to a negative peak. The magnitudes of both positive and negative peaks in exposure II are the second largest among all the tested exposure cases. The aerodynamic damping ratio in the vicinity of a reduced wind speed of 14 tends to first increase and then decrease. However, the magnitude of the increase in exposure II is much smaller than that in exposure I. In exposures III to VII, the aerodynamic damping ratio also changes rapidly from a positive peak to a negative peak when the reduced wind speed is varied from 7 to 12. The magnitudes of the positive and negative peaks decrease with increasing turbulence intensity. In exposures III to VI, aerodynamic damping ratios at low reduced wind speeds are positive while that at high reduced wind speeds are negative. However, the aerodynamic damping ratio increases to a positive value at about reduced wind speed of 11 in exposure VII. The aerodynamic damping ratios at all the tested reduced wind speeds are positive in exposure VIII, in which turbulence intensities are the highest ones. The variation of the aerodynamic damping ratios with the wind speed variation is smaller in this exposure case than those in other exposures with lower turbulence intensities. Generally, the exposure has a remarkable effect on the aerodynamic damping ratio. The magnitudes of both the positive and negative peaks decrease with increasing turbulence intensity, while the critical reduced wind speed increases with the turbulence intensity.

According to Cao (2012), the across-wind aerodynamic damping ratio is inversely proportional to the tip deflection at low reduced wind speed in trubulence flows. The change of exposure simultaneously induces the change of turbulence intensity at the model height and wind-induced response (dimensionless tip deflection X/B, where X is RMS of wind-induced displacement response). To eliminate the interference of varying tip deflection, the ordinate ζ_a in Fig. 8(a) was replaced by $X/B \times \zeta_a$ to obtain the variation curve of $X/B \times \zeta_a$ with reduced wind speed, as shown in Fig. 8(b). Fig. 8(b) indicates that $X/B \times \zeta_a$ increases with turbulence intensity in exposures I to III, and decreases basically with increasing turbulence intensity in exposures III to VIII when the reduced wind speed is lower than the critical reduced wind speed.

At the same time, the critical reduced wind speed for $X/B \times \zeta_a$ from positive value to negative value increases with turbulence intensity. This trend is believed to be related to the bigger Strouhal frequency for larger turbulence intensity, which induces a vortex-excited resonance to occur at a higher reduced wind speed. In the vicinity of the critical reduced wind speed for vortex-induced resonance, the magnitude of $X/B \times \zeta_a$ reaches a large negative peak in exposures with relatively lower turbulence intensities, such as exposures I, II, and III. However, no negative peak is observed near the critical reduced wind speed in exposures with relatively higher turbulence intensities, such as exposures IV, V, and VI. A small peak, either positive or negative, exists around the critical reduced wind speed of vortex induced resonance in exposures with very high turbulence intensities, such as exposures VII and VIII.

Moreover, $X/B \times \zeta_a$ increases at first and then decreases as the reduced wind speed increases above the critical wind speed .Combining these results with those by Cheng (2002) show that even if the mass-damping coefficient of a model is fixed, its aerodynamic stability is also different in different wind flow conditions, thus inducing significant discrepancies in the aerodynamic damping ratios between one another.

4.2 Effect of aspect ratio H/B

Fig. 9(a) shows the variations of aerodynamic damping ratio ζ_a with reduced wind speed U_H/f_0B for aspect ratios H/B ranging from 5 to 10 and a side ratio B/D of 1 in exposure B. As shown in Fig 9(a), the aerodynamic damping ratio increases with treduced wind velocity and reaches a positive peak at the reduced wind speed of approximately 7. The magnitudes of the positive peaks for models with an aspect ratio of 8 and 10 are very close to each other, whereas the magnitude of positive peak for the aspect ratio of 5 is much smaller. This difference may be related to the discrepant tip deflection caused by the amplitude-dependent structural damping ratio. When reduced wind speed is varied from 7 to 10, the aerodynamic damping ratio undergoes a rapid sign change from a positive to a negative peak. Aerodynamic damping ratios for the aspect ratio of 5 at reduced wind speeds higher than 10 are not presented in the figure because of the limitation of the maximum working wind speed of the wind tunnel. Meanwhile, the aerodynamic damping ratios for the aspect ratios of 8 and 10 at high reduced wind speeds are very close to each other.

In this study, the model heights were remained a fixed value while the width and length were changed to achieve a variation of the aspect ratio. The change of aspect ratio simultaneously induces the change of wind-induced response (dimensionless tip deflection X/B).

The variation curve of $X/B \times \zeta_a$ with reduced wind speed $U_H/(f_0B)$ can eliminate the interference of varying tip deflection. In this way, the effect of aspect ratio on the aerodynamic damping ratio can be investigated independently. Accordingly, ordinate ζ_a in Fig. 9(a) is replaced by $X/B \times \zeta_a$ to obtain the variation curve of $X/B \times \zeta_a$ with reduced wind velocity, as shown in Fig. 9(b). Fig. 9(b) indicates that $X/B \times \zeta_a$ for various aspect ratios at a certain reduced wind speed close to one another. This finding is not totally consistent with the effect of aspect ratio on aerodynamic damping ratio presented by Marukawa (1996) and Steckley (1989).

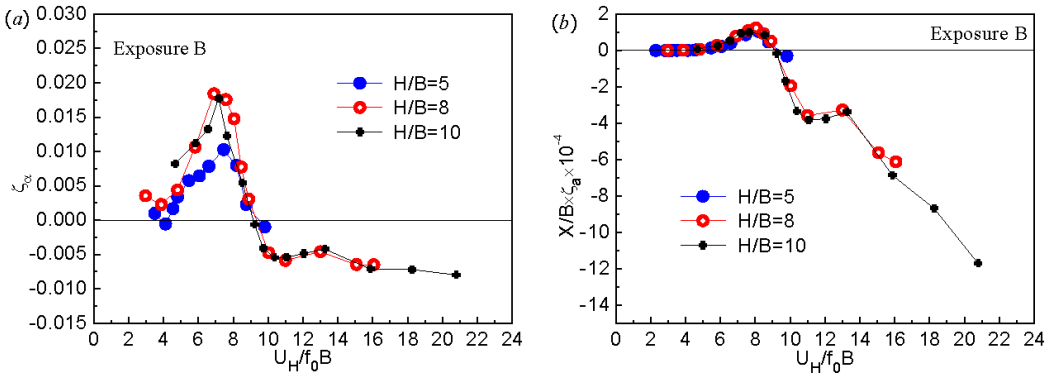

Fig. 9 Effect of aspect ratio H/B on across-wind aerodynamic damping ratio ζ_a

It is because both the aeroelastic experimental study of Marukawa (1996) and the forced vibration experimental study of Steckley (1989) fixed the breadth and depth and changed the height of the model to achieve a variation of the aspect ratio. The effects of aspect ratio was failed to be examined individually because turbulence intensity at model height was changed with the change of aspect ratio. Thus, test results exhibited the interference of turbulence intensity. And turbulence intensity has a significant effect on the aerodynamic damping ratio. Therefore, existing studies cannot exactly reflect the effect of aspect ratio on aerodynamic damping ratio. In conclusion, aspect ratio has a minimal effect on the value of $X/B\times\zeta_a$ at a certain reduced wind speed.

4.3 Effect of side ratio B/D

Fig. 10(a) shows the variations of aerodynamic damping ratio ζ_a with reduced wind speed U_H/f_0B for an aspect ratio $H/(BD)^{0.5}$ of 8 and side ratios B/D varying from 0.33 to 3 in exposure B. As shown in Fig. 10(a), side ratio has remarkable influence on across-wind aerodynamic damping ratio.

Completely different variation regularities are observed for B/D<1, B/D=1, and B/D>1, which is believed to be related to whether reattachment occurs and to the reduced wind speed at which reattachment occurs for corresponding case. For side ratios B/D<1, aerodynamic damping ratios are positive for all tested reduced wind speeds, and aerodynamic damping ratio increases monotonically with reduced wind speed in most cases. Zigzags are observed at reduced wind speeds of 14 and 21. At the same time, the aerodynamic damping ratio decreases with the side ratio for all reduced wind speeds, which can be attributed to the significant reattachment for smaller side ratio. For side ratio B/D=1, the aerodynamic damping ratio is positive at low reduced wind speeds, and the magnitude increases with reduced wind speed. When reduced wind speed is higher than 7, the aerodynamic damping ratio generally decreases as reduced wind speed increases. When reduced wind speed is varied from 7 to 11, the aerodynamic damping decreases rapidly and its sign changes at a reduced wind speed of approximately 9. For side ratios B/D>1, aerodynamic damping ratio monotonically decreases as reduced wind speed increases when reduced wind speed is lower than 8.5. In these cases, no obvious positive peak is observed, and only a zigzag is exhibited at a reduced wind speed of 4. The aerodynamic damping ratio undergoes a sign change from a positive peak to a negative peak at a reduced wind speed approximately 4.5, which is far below the onset reduced wind speed for galloping.

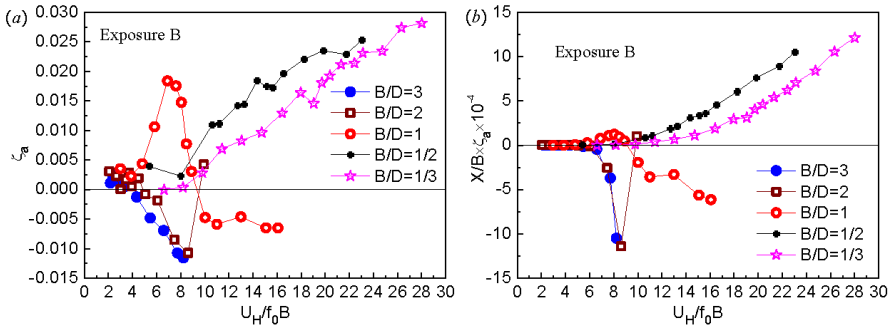

Fig. 10 Effect of side ratio B/D on across-wind aerodynamic damping ratio ζ_a

Notably, the increment of the aerodynamic damping ratio from a great negative value to a positive value is very large when reduced wind speed is varied from 8.5 to 10 for a side ratio of 2. Steckley (1989) has also estimated aerodynamic damping ratios at high reduced wind speeds for a side ratio of 2 from forced vibration experiments. Compared with the results of Steckley (1989), the aerodynamic damping ratio should increase with reduced wind speed between 8.5 and 10 and then decrease with increase of reduced wind speed, but the variation regularity of aerodynamic damping ratios at high reduced wind speeds still need further research.

In this part, the mean aspect ratio $H/(BD)^{0.5}$ was remained the same while the side ratio was changed, such that the aspect ratio H/B was changed. From the discussion above, we can see that aspect ratio has a minimal effect on the aerodynamic damping ratio. In addition, the across-wind aerodynamic damping ratio is inversely proportional to tip deflection at low reduced wind speed in turbulent flows, as reported by Cao (2012). To eliminate the interference of varying tip deflection, the ordinate ζ_a should be replaced by $X/B \times \zeta_a$. Fig. 10(b) shows the variation curve of $X/B \times \zeta_a$ with reduced wind speed to examine individually the effect of the side ratio. Fig. 10(b) indicates that the variation of $X/B \times \zeta_a$ with reduced wind speed is similar to that of ζ_a when the side ratios B/D are below 1. At the same time, $X/B \times \zeta_a$ increases with the side ratio because a smaller side ratio results in a more significant effect of reattachment, thus reducing the interaction effect between the wind and the structure. The same tendency as ζ_a is observed for $X/B \times \zeta_a$ when the side ratio is 1. The values for cases with side ratios B/D greater than 1 are very close to one another at a reduced wind speed lower than 4.5. For $B/D>1$, $X/B \times \zeta_a$ changes from a near-zero value to a maximum negative value and then returns to a near-zero value when reduced wind speed is varied from 4.5 to 8.5. Meanwhile, the discrepant of $X/B \times \zeta_a$ between cases with side ratios of 2 and 3 is very small. The aerodynamic damping ratio for the case with a side ratio of 3 at a reduced wind speeds above 8.5 is not presented because of the limitation of the maximum working wind speed of the wind tunnel. Moreover, only one value of $X/B \times \zeta_a$ is obtained for the case with a side ratio of 2 at wind speeds higher than 8.5. In summary, side ratio has a significant effect on aerodynamic damping ratio as completely different variations are observed for B/D<1, B/D=1, and B/D>1.

5. Formula fitting of aerodynamic damping ratio

According to the experimental study of the effects of structural dynamic characteristics on the across-wind aerodynamic damping of square super-high-rise buildings presented by Cao (2012), the empirical aerodynamic damping function proposed to estimate the across-wind aerodynamic damping ratios at low reduced wind speeds for square high-rise buildings with an aspect ratio of 8 in terrain category B (turbulence intensity at model height is 9.36%) is

$$\zeta_a = \frac{0.0389\, R_V^5 \left(0.89^2 - R_V^2\right)}{\left(1 - R_V\right)^2 + 0.181 R_V^{4.447}} \frac{\rho_a}{\rho_s} \frac{B}{X}, \quad (R_V \le 1) \tag{2}$$

where $R_V = V_m/V_s$; V_m is the reduced wind speed of oscillating prism [$V_m=U_H/(f_0B)$]; V_s is the reduced wind speed for Strouhal frequency [$V_s=U_H/(f_sB)$]; mass ratio ρ_a/ρ_s is the ratio of air density to mass density of prism; and dimensionless tip deflection X/B is the ratio of wind-induced displacement response X to model width B. The empirical aerodynamic damping function proposed to evaluate the across-wind aerodynamic damping ratios at high reduced wind speeds for high-rise buildings with an aspect ratio of 8 in terrain category B is

$$\zeta_a = \zeta_s\left(A_H e^{-S_H(\ln(R_H/P_H))^2} + F_p + F_0\right), \quad (R_V>1) \tag{3}$$

where $R_H = R_V-1$; A_H is a parameter related to the magnitude of the function; S_H is a parameter related to the sharpness of the function; P_H is a parameter related to the peak position of the function; F_p is a term introduced from Parkinson's quasi-steady theory (Parkinson 1963) and is expressed in the form of mass-damping parameter, with $F_p = \alpha R_H = (-0.5/R_{Hg})R_H = -R_H/\{2(V_{mg}/V_s-1)\}$; V_{mg} is the critical reduced wind speed for galloping as $V_{mg} = (8\pi/3)(1/C'_{FY})(\rho_s/\rho_a)\zeta_s$; C'_{FY} is the first-order derivative of generalized aerodynamic force coefficient to wind angle; and F_0 is the initial value of the function.

From Eqs. (2) and (3), we can see that formula fitting and the study of the variation regularity of the aerodynamic damping ratio all greatly related to V_s. Quan (2002) proposed a fitting equation for V_s as

$$f_s = 10^{-5}(191-9.48\alpha_w+1.28\alpha_{hr}+\alpha_{hr}\alpha_w)(68-21\alpha_{db}+3\alpha_{db}^2) \tag{4}$$

where $\alpha_{hr}=H/(BD)^{0.5}$; $\alpha_{db}=D/B$; α_w=1(A), 2(B), 3(C), 4(D); and A, B, C, and D respectively represent the terrain categories A, B, C, and D provided in the Chinese code. According to Eq. (4), V_s is separately 10.01, 10.09, 10.16, and 10.24 for the standard model with α_{hr} of 8 and α_{db} of 1 in terrain categories A, B, C, and D, which are very close to one another. This condition can be attributed to the fact that the longitudinal turbulence intensities of terrain categories A, B, C, and D at building height are very close to one another with values of 9.23%, 9.36%, 9.52%, and 9.78%, respectively, which are simulated according to the Chinese code and AIJ (2004). Moreover, the effect of the mean wind speed profile on aerodynamic damping ratio is minimal. Hence, Eq. (4) does not take sufficient consideration of the effect of exposure (turbulence intensity). Based on Eq. (4) and combined with the effect of turbulence intensity ranging from 1.73% to 24.92% on V_s in this study, the following improvements are made on Eq. (4).

For terrain category B with a simulated turbulence intensity of 9.36%, V_{sB} is 10.087 according to Eq. (4). According to the PSDs of wind-induced responses obtained from related experiments, V_s is 9.5, 9.7, 10.0, 10.1, 10.2, 10.2, 10.5, and 10.9 for exposures I to VIII, respectively. Improvements on the estimation of V_s based on Eq. (4) require the normalization of V_s for the exposures, i.e., V_s/V_{sB}=[0.942, 0.962, 0.991, 1.001, 1.011, 1.011, 1.0410, 1.081] for exposures I to VIII, respectively. The primary fitting equation of V_s/V_{sB} with I_u is obtained by using the least square method as

$$V_s / V_{sB} = 0.42 \times I_u^{0.68} + 0.915 \tag{5}$$

Combining Eqs. (4) and (5), Eq. (6) is derived. The parameter α_{db} ($\alpha_{db}=D/B$) in Eq. (4) is replaced by α_{bd} ($\alpha_{bd}=B/D$) considering the parameter adopted in this paper.

$$V_s = 10^4\left(4.2\times I_u^{0.68}+9.15\right)\left(172+3.3\alpha_{hr}\right)^{-1}\left(68-21\alpha_{bd}^{-1}+3\alpha_{bd}^{-2}\right)^{-1} \tag{6}$$

Fig. 11 shows the variation curve of V_s obtained from the experiment with turbulence intensity I_u at building height. The conformity between V_s derived from the wind tunnel test and V_s calculated by the fitting Eq. (6) is also shown in Fig. 11. The total standard error for this empirical equation is

$$\delta_{V_s} = \sqrt{\frac{1}{N}\sum_{i=1}^{N}\left(V_{s-calc}(i) - V_{s-test}(i)\right)^2} = 0.0532$$

where N=8 is the number of test cases; and V_{s-calc} and V_{s-test} are the tested and fitted values for V_s, respectively.

5.1 Effect of exposure

As shown in Fig. 8(b), different turbulence intensities induce discrepant magnitudes of aerodynamic damping ratios. Based on the physical meanings of the parameters of Eq. (2) and combined with the effect of turbulence intensity on aerodynamic damping ratio, Eq. (2) for low reduced wind speed is rewritten as

$$\zeta_a = \frac{A_L R_V^5 \left(0.89^2 - R_V^2\right)}{\left(1 - R_V\right)^2 + S_L R_V^{E_L}} \frac{\rho_a}{\rho_s} \frac{B}{X}, \quad (R_V \leq 1) \tag{7}$$

where A_L is a parameter related to the magnitude of positive peak; S_L is a parameter related to sharpness; and E_L is a parameter related to the magnitude of negative peak. The values of A_L, S_L, and E_L for all the cases can be derived by parameter fitting of Eq. (7). Fig. 12 shows the primary fitting and secondary fitting variation curves of positive magnitude parameter A_L, sharpness parameter S_H, and the negative magnitude parameter E_L with turbulence intensity I_u. The secondary fitting equations are

$$A_L = -0.34\ln(0.96I_u) + 0.06 \tag{8}$$

$$S_L = 93.1 \times I_u^2 - 9.7I_u + 2.0 \tag{9}$$

$$E_L = 125.76I_u^{0.0822} - 49.94I_u - 100 \tag{10}$$

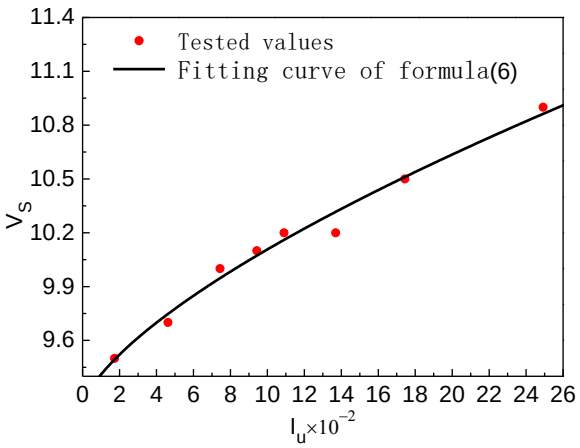

Fig. 11 Relationship between Vs and Iu

Fig. 13 shows the conformity between ζ_a derived from the wind tunnel test and those obtained by the fitting Eq. (7) combined with Eqs. (8)-(10). The total standard error $\delta_{\zeta a}$ for these empirical equations is

$$\delta_{\zeta a}=\sqrt{\frac{1}{N}\sum_{i=1}^{N}\left(\zeta_{a-calc}(i)-\zeta_{a-test}(i)\right)^2}=4.55\times10^{-3}$$

where the total number N of test speeds for all the cases is 178; and $\zeta_{a\text{-}calc}$ and $\zeta_{a\text{-}test}$ are respectively the tested values and fitted values for aerodynamic damping ratio. The values of A_L, S_L, E_L, V_s obtained by Eq. (8), (9), (10) and (6), standard error $\delta_{\zeta ai}$ and number N_i of test speeds for each case are shown in Table 4.

Fig. 14 shows variation curve of ζ_a/ζ_s with relative reduced wind speed V_m/V_s in exposures I to VIII. As shown in Fig. 14, V_m/V_s corresponding to the positive peak of ζ_a/ζ_s decreases from exposure I to exposure VIII. The values of ζ_a/ζ_s for all the cases at V_m/V_s of 0.9 are almost the same, nearly zero.

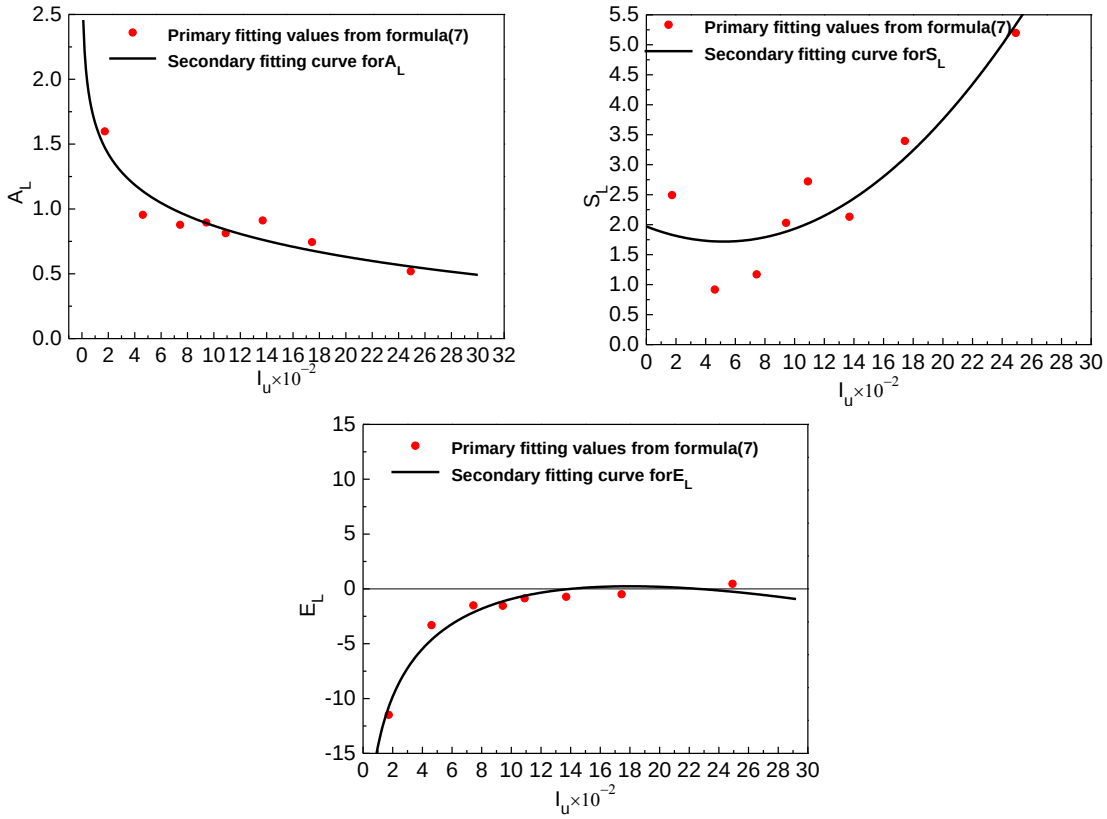

Fig. 12 Relationship between fitted parameters (A_L, S_L and E_L) and I_u

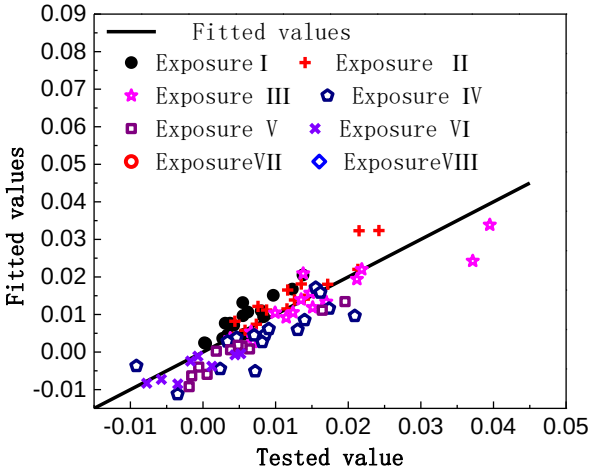

Fig. 13 Comparison between fitted and tested values of aerodynamic damping ratios at low reduced speeds for high-rise buildings in various wind conditions

Table 4 Fitted parameters of aerodynamic damping ratios at low reduced speeds for high-rise buildings in various wind conditions

Exposure	I	II	III	IV	B	V	VI	VII	VIII
A_L	1.45328	1.11930	0.95730	0.87671	0.87925	0.82746	0.74972	0.66766	0.54631
S_L	1.86005	1.75058	1.79366	1.91318	1.87773	2.04882	2.41849	3.13999	5.36433
E'_L	-10.767	-4.634	-2.140	-1.136	-1.164	-0.629	-0.039	0.234	-0.258
V_s	9.492	9.747	9.947	10.074	10.061	10.162	10.320	10.515	10.870
$\delta_{\zeta ai}$ ($\times 10^{-3}$)	5.08	12.32	9.63	2.72	0.12	5.75	2.53	2.94	2.22
N_i	8	9	10	11	95	11	11	12	11

The magnitude of the negative peak of ζ_a/ζ_s at approximately V_m/V_s=1 decreases with increasing turbulence intensity. For high reduced wind speeds, Eq. (11) is derived according to the physical meanings of the parameters of Eq. (3). The parameter α of $F_p=\alpha R_H$ is taken as an fitted parameter considering that no stipulations are provided in the related specifications and no experimental data are measured for C'_{FY}.

$$\zeta_a = \zeta_s\left(A_H e^{-S_H(\ln(R_H/P_H))^2} + \alpha R_H + F_0\right), (R_V>1) \tag{11}$$

where the physical meanings of the parameters are all the same as those in Eq. (3). Here, F_0 = [-1, -0.9, -0.8, -0.6, -0.5, -0.3, 0, 0.1] for exposures I to VIII. The conformity between the value of ζ_a obtained from the wind tunnel test with that derived by Eq. (11) is shown in Fig. 15. The total

standard error $\delta_{\zeta a}$ for these empirical equations is 1.111×10^{-3}. The total number N of test speeds for all the cases is 47. The values of A_H, S_H, P_H, α, F_0, standard error $\delta_{\zeta ai}$ and number N_i of test speeds for each case are shown in Table 5. Only a few values are tested for high reduced wind speed. Thus, no unified fitting for regularity is made in this work, and the fitted parameters for each case merely provide references for structural design engineers when similar exposure is simulated.

5.2 Effect of aspect ratio

The aspect ratio not only has a minimal effect on $X/B\times\zeta_a$ at low reduced wind speed, but also has a limited effect on ζ_a/ζ_s at high reduced wind speed.

Table 5 Fitted parameters of aerodynamic damping ratios at high reduced wind speeds for high-rise buildings in various wind conditions

Exposure	I	II	III	IV	V	VI	VII	VIII
A_H	3.508	0.0168	-0.175	-0.317	0.143	0.210	0.263	0.425
S_H	4.694	2.149	0.0710	0.210	4.130	0.616	0.582	0.455
P_H	0.320	0.320	0.320	0.320	0.320	0.320	0.320	0.320
α	2.513	0.763	0.0394	-0.114	-0.692	-0.538	-0.361	0.00425
F_0	-1	-0.9	-0.8	-0.6	-0.5	-0.3	0	0.1
$\delta_{\zeta ai}$ ($\times10^{-3}$)	1.880	1.849	0.126	0.134	0.249	0.517	0.847	0.639
N_i	7	8	8	7	6	3	4	4

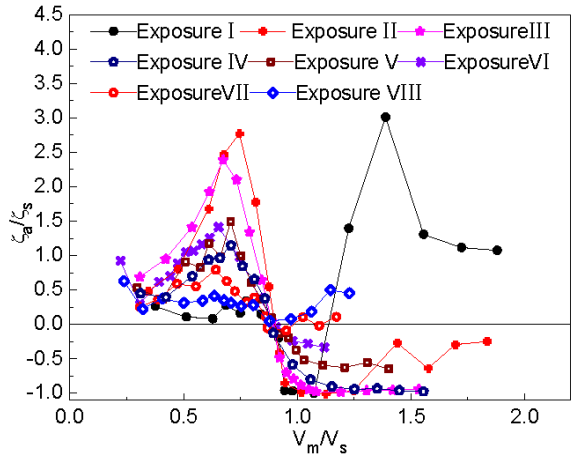

Fig. 14 Effect of roughness exposure on ζ_a/ζ_s

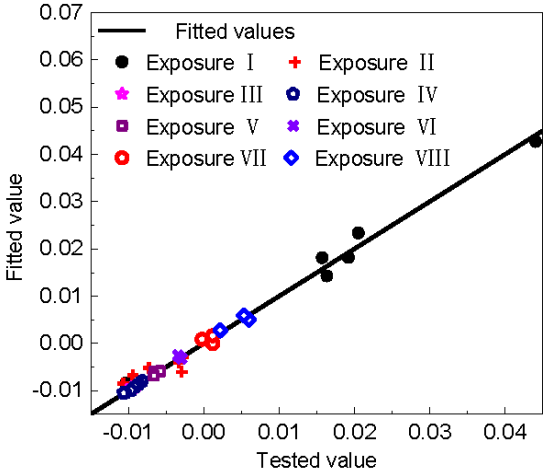

Fig. 15 Comparison between fitted and tested values of aerodynamic damping ratios at high reduced wind speeds for high-rise buildings in various wind conditions

The empirical aerodynamic damping function for square high-rise buildings with an aspect ratio of 8 in terrain category B proposed by Cao (2012), i.e., Eqs. (2) and (3) in this paper, can thus be developed to estimate the aerodynamic damping ratios for all tall square buildings with various aspect ratios in terrain category B. For aspect ratios of 5 and 10, V_s is 10.722 and 9.859, respectively, as calculated by Eq. (6). In addition, according to the experiment conducted by Wu (2012), aspect ratio has a minimal effect on the first-order derivative of the generalized aerodynamic force coefficient to wind angle C'_{FY} for square high-rise buildings.

5.3 Effect of side ratio

As shown in Fig. 10(b), side ratio has a significant effect on aerodynamic damping ratio as completely different variations of aerodynamic damping ratio with reduced wind speed are observed for $B/D<1$, $B/D=1$, and $B/D>1$. Sections 5.1 and 5.2 have already presented the empirical aerodynamic damping functions for tall square buildings. Thus, only cases with side ratios not equal to 1 are discussed here. First, V_s is separately 8.209, 8.643, 10.070, 13.249, and 15.734 for side ratios of 3, 2, 1, 1/2 and 1/3, which are obtained by Eq. (6). The variation curve of $X/B\times\zeta_a\times\rho_s/\rho_a$ with V_m/V_s is shown in Fig. 16.

Fig. 16 indicates that the R_V value from which aerodynamic positive damping changes to negative damping for side ratio bigger than 1 is approximately 0.5, and R_V value at which negative peak of aerodynamic damping ratio occurs is approximately 1. For side ratios smaller than 1, aerodynamic damping ratios are all positive, and no peak value is observed within the tested wind speed range. However, a positive peak of aerodynamic damping ratio may occur at a higher reduced wind speed based on Steckley (1989).

At low reduced wind speeds, Eq. (12) is derived based on the physical meanings of the parameters of Eq. (7) and combined the effect of side ratio.

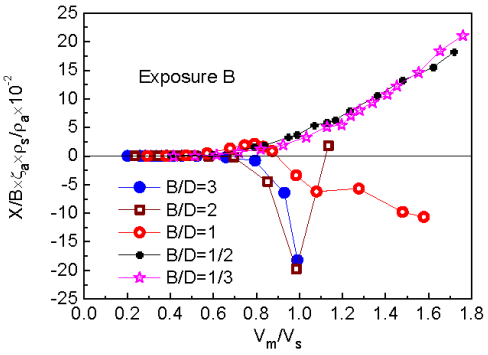

Fig. 16 Effect of side ratio on $X / B \times \zeta_a \times \rho_s / \rho_a$

$$\zeta_a = \frac{A_L R_V^5 \left(C_L^2 - R_V^2\right)}{\left(1-R_V\right)^2 + S_L R_V^{E_L}} \frac{\rho_a}{\rho_s} \frac{B}{X}, \quad (R_V \leq 1) \tag{12}$$

where C_L is the critical reduced wind speed ratio, of which the physical meaning is the R_V at which aerodynamic positive damping ratio changes to negative damping. The physical meanings of other parameters in Eq. (12) are the same as those in Eq. (7). The values of A_L, C_L, S_L, and E_L for all the cases can be derived through the parameter fitting of Eq. (12). After numerous comparisons, the secondary fitting equations for A_L, C_L, S_L, and E_L are derived as

$$A_L = -0.0712 e^{-0.42\left(\log\left(\alpha_{bd}/0.31\right)\right)^4} + 0.07134 \tag{13}$$

$$C_L = 0.385 \alpha_{bd}^{-3} + 0.505 \tag{14}$$

$$S_L = \begin{cases} -0.619\,\alpha_{bd} + 0.8 & (\alpha_{bd} \leq 1) \\ 0.0538\,\alpha_{bd} + 0.133 & (\alpha_{bd} > 1) \end{cases} \tag{15}$$

$$E_L = \begin{cases} 6.572\,\alpha_{bd} - 2.125 & (\alpha_{bd} \leq 1) \\ -5.069\,\alpha_{bd} + 9.516 & (\alpha_{bd} > 1) \end{cases} \tag{16}$$

Fig. 17 shows the conformity between ζ_a derived from the wind tunnel test and those obtained by fitting Eq. (12) combined with Eqs. (13) to (16). The total standard error $\delta_{\zeta a}$ for these empirical equations is 1.632×10^{-3}. The total number N of test speeds for all the cases is 47. The values of A_L, S_L, E_L, C_L, V_s obtained by Eq. (6), standard error $\delta_{\zeta ai}$ and number N_i of test speeds for each case are shown in Table 6.

For side ratios greater than 1, only one value is tested at high reduced wind speed. Thus, research on the variation regularity of these cases is not performed in this work. When the side ratios are smaller than 1, aerodynamic damping ratios at high reduced wind speeds can also be estimated by Eqs. (12) to (16). The conformity between the aerodynamic damping ratios obtained from the wind tunnel test and that derived by the fitting equations is also presented in Fig. 17. The total standard error $\delta_{\zeta a}$ for these empirical equations is 1.100×10^{-3}. The total number N of test speeds for all the cases is 19.

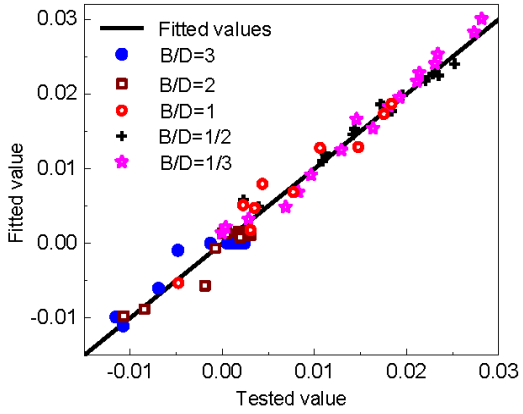

Fig. 17 Comparison between fitted values and tested values of aerodynamic damping ratios for high-rise buildings with various side ratios

Table 6 Fitted parameters of aerodynamic damping ratios for high-rise buildings with various side ratios

B/D	3	2	1	1/2	1/3
A_L	0.0713	0.0709	0.0389	0.00167	0.000137
C_L	0.519	0.553	0.890	3.585	10.924
S_L	0.295	0.241	0.181	0.491	0.594
E_L	-5.703	-0.622	4.447	1.161	0.0640
V_s	8.305	8.744	10.187	13.404	15.918
$\delta_{\zeta ai}$ ($\times 10^{-3}$)	1.704	1.486	1.832	1.614	1.400
N_i	13	12	10	6	6

5.4 Synthesis of fitting formulas

When the reduced wind speed of incident flow is lower than it critical value for vortex excited resonance, a combination of Eqs. (2), (6)-(10), and (12)-(16) derive the aerodynamic damping functions for rectangular super-high-rise buildings with various aspect ratios, side ratios, and turbulence intensities.

$$\zeta_a = \frac{A_L R_V^5 \left(C_L^2 - R_V^2\right)}{\left(1 - R_V\right)^2 + S_L R_V^{E_L}} \frac{\rho_a}{\rho_s} \frac{B}{X}, \quad (\mathrm{R_V} \le 1) \tag{17}$$

$$A_L = (-0.34 \ln(0.96 Iu) + 0.06)\left(-0.0712 e^{-0.418\left(\log(\alpha_{bd}/0.31)\right)^4} + 0.071336\right) \tag{18}$$

$$C_L = 0.385\alpha_{bd}^{-3} + 0.505 \tag{19}$$

$$S_L = \begin{cases} \left(93.1\times I_u^2 - 9.7I_u + 2.0\right)\left(-0.619\alpha_{bd} + 0.8\right) & (\alpha_{bd} \le 1) \\ \left(93.1\times I_u^2 - 9.7I_u + 2.0\right)\left(0.0538\alpha_{bd} + 0.133\right) & (\alpha_{bd} > 1) \end{cases} \tag{20}$$

$$E_L = \begin{cases} \left(125.76I_u^{\,0.0822} - 49.94I_u - 100\right)\left(6.572\alpha_{bd} - 2.125\right) & (\alpha_{bd} \le 1) \\ \left(125.76I_u^{\,0.0822} - 49.94I_u - 100\right)\left(-5.069\alpha_{bd} + 9.516\right) & (\alpha_{bd} > 1) \end{cases} \tag{21}$$

$$V_s = 10^4\left(4.2\times I_u^{0.68} + 9.15\right)\left(172 + 3.3\alpha_{hr}\right)^{-1}\left(68 - 21\alpha_{bd}^{-1} + 3\alpha_{bd}^{-2}\right)^{-1} \tag{22}$$

The total standard error $\delta_{\zeta a}$ for these empirical equations is 3.63×10^{-3}. These equations are suitable for tall rectangular buildings when turbulence intensity I_u is varied from 1.73% to 24.92%, the mean aspect ratio α_{hr} ranges from 5 to 10, and side ratio α_{bd} is 1/3 to 3.

When reduced wind speed of incident flow is higher than it critical value for vortex excited resonance, the empirical aerodynamic damping function is

$$\zeta_a = \zeta_s\left(A_H e^{-S_H\left(\ln(R_H/P_H)\right)^2} + F_p + F_0\right), \quad (R_V>1) \tag{23}$$

Parameters are adopted the fitted values for corresponding cases.

6. Conclusions

The effects of aspect ratio, side ratio, and turbulence intensity of incident flow on across-wind aerodynamic damping ratios are investigated with a series of aeroelastic model wind tunnel tests. The following conclusions can be achieved from this research:

- Exposure category (turbulence intensity I_u) has a significant effect on aerodynamic damping ratio ζ_a. The magnitudes of the positive and negative peaks basically decrease with the increase of turbulence intensity.
- The aspect ratio itself has almost no effect on $X/B\times\zeta_a$. In fact, it affects the response amplitude of buildings and thus indirectly affects aerodynamic damping ratio. So there is the parameter of building response amplitude but not the parameter of aspect ratio as an argument in the fitted empirical equations of aerodynamic damping.
- Side ratio has significant effects on across-wind aerodynamic damping ratio. For B/D<1, B/D=1 and B/D>1, the variation patters of the across-wind aerodynamic damping ratio are completely different.
- Empirical aerodynamic damping functions (17)-(22) and (23) are proposed to estimate the across-wind aerodynamic damping ratios at low and high reduced wind speeds for rectangular high-rise buildings with various side ratios,urbulence intensities and response amplitudes.

Acknowledgements

The authors gratefully acknowledge the support of the National Natural Science Foundation of China (51278367, 90715040, 91215302).

References

AIJ 2004 (2004), *Recommendations for Loads on Building*, Architectural Institute of Japan.

Aquino, R.E.R. and Tamura, Y. (2011), "Damping based on EPP spring models of stick-slip surfaces", *Proceedings of the 13th ICWE*, Amsterdam, Holland, July.

Cao H.L. (2012), *Aerodynamic damping of super-high-rise building*, Ph.D Thesis (in Chinese), Tongji University, Shanghai, China.

Cheng, C.M., Lu, P.C. and Tsai, M.S. (2002), "Across-wind aerodynamic damping of isolated square-shaped buildings", *J. Wind Eng. Ind. Aerod.*, **90**(12-15), 1743-1756.

Davenport, A.G. (1979), "The influence of turbulence on the aeroelastic responses of tall structures to the wind", *IAHR-IUTAM Symp. Pract. Exp. with Flow Ind. Vib.*, Karlsruhe, Germany, July.

GB50009-2001(2012), *Load Code for the Design of Building Structures* (in Chinese), China Architecture & Building Press.

Gu, M. and Quan, Y. (2004), "Across-wind loads of typical tall buildings", *J. Wind Eng. Ind. Aerod*., **92**(13), 1147-1165.

Kareem, A. (1978), *Wind excited motion of buildings*, Ph.D thesis, Colorado State University at Fort Collin, Colorado, USA.

Kim, Y.C., Tamura, Y. and Yoon, S.(2015), "Effect of taper on fundamental aeroelastic behaviors of super-tall buildings", *Wind Struct*., **20**(4), 527-548.

Li Q.S., Hu G. and Yan B. (2014), "Investigation of the effects of free-stream turbulence on wind-induced responses of tall building by Large Eddy Simulation", *Wind Struct*., **18**(6), 599-618

Marukawa, H., Kato, N., Fujii, K. and Tamura, Y. (1996), "Experimental evaluation of aerodynamic damping of tall buildings", *J. Wind Eng. Ind. Aerod.*, **59**(2-3), 177-190.

Nishimura, H. and Taniike, Y. (1995), "Unsteady wind forces on a square prism in a turbulent boundary layer", *Proceedings of the 9th ICWE*, New Delhi, India, July.

Okada, K., Nakamura, Y., Shiba, K., Hayakawa, T., Tsuji, E. and Ukita, T. (1993), *Forced vibration tests of ORC200 symbol Tower, Part 1: Test methods and results*, Summaries of technical Papers of Annual Meeting of Architectural Institute of Japan, Structures 1, 875-876.

Parkinson, G.V. (1963), "Aeroelastic galloping in one degree of freedom", *Proceedings of the Symp On Wind Effects on Buildings and Structures*, Teddington, England, July.

Quan, Y. (2002), Across-wind loads and responses on super high-rise buildings, Ph.D. Thesis (in Chinese), Tonji University, Shanghai, China.

Quan, Y. and Gu, M. (2004), "Aerodynamic damping of square section high-rise buildings" (in Chinese), *J. Eng. Mech., China Society of Theoretical and Applied Mechanics*, **21**(1), 26-30.

Quan, Y. and Gu, M. (2005), "Experimental evaluation of aerodynamic damping of square super high-rise buildings", *Wind Struct.*, **8**(5), 309-324.

Steckley, A. (1989), *Motion-Induced Wind Forces on Chimneys and Tall Buildings*, Ph.D thesis, The University of Western Ontario, London, Ontario, Canada.

Steckley, A., Vickery, B.J. and Isyumov, N. (1990), "On the measurement of motion induced forces on models in turbulent shear flow", *J. Wind Eng. Ind. Aerod.*, **36**(1-3), 339-350.

Tamura, Y. (2006), "Amplitude dependency of damping in buildings and estimation techniques", *Proceedings of the 12th AWES Wind Engineering Workshop*, Queenstown, New Zealand, August.

Tamura, Y., Suda, K. and Sasaki, A. (2000), "Damping in buildings for wind resistant design", *Proceedings of the International Symposium on Wind and Structures for the 21st Century*, Cheju, Korea, July.

Tamura, Y. and Suganuma, S.Y. (1996), "Evaluation of amplitude-dependent damping and natural frequency of buildings during strong winds", *J. Wind Eng. Ind. Aerod.*, **59** (2-3), 115-130.
Vickery, B.J. and Steckley, A. (1993), "Aerodynamic damping and vortex excitation on an oscillating prism in turbulent shear flow", *J. Wind Eng. Ind. Aerod.*, **49**(1-3), 121-140.
Venanzi, I. and Materazzi, A.L. (2012), "Acrosswind aeroelastic response of square tall buildings: a semi-analytical approach based of wind tunnel tests on rigid models", *Wind Struct*., **15**(6), 495-508.
Watanabe, Y., Isyumov, N. and Davenport, A.G. (1997), "Empirical aerodynamic damping function for tall buildings", *J. Wind Eng. Ind. Aerod.*, **72**(1-3), 313-321.
Wu, D. (2012), *Research on across-wind galloping stability of high-rise buildings with rectangular cross-sections*, Master Thesis (in Chinese), Tongji University, Shanghai, China.
Zou, L.H., Liang, S.G. and Gu, M. (2003), "Evaluation of aerodynamic damping in wind-induced vibration of tall buildings by random decrement technology", *J. HU ST. (Urban Science Edition)*, **20**(1), 30-33 [In Chinese].

CC